Electronic Supplementary Material (ESI) for Materials Horizons.

Supplementary Information

Origin of anisotropic-strain-driven photoresponse enhancement in inorganic-halide-based self-powered flexible photodetectors

Da Bin Kim,[a] Ju Han,[a] Ye Seul Jung,[a] Kwan Sik Park,[a] Youngseo Park,[b] Junseok Heo[b] and Yong Soo Cho*[a]

[a]Department of Materials Science and Engineering, Yonsei University, Seoul 03722, Korea
[b]Department of Electrical and Computer Engineering, Ajou University, Suwon 16499, Korea

*Corresponding author: ycho@yonsei.ac.kr

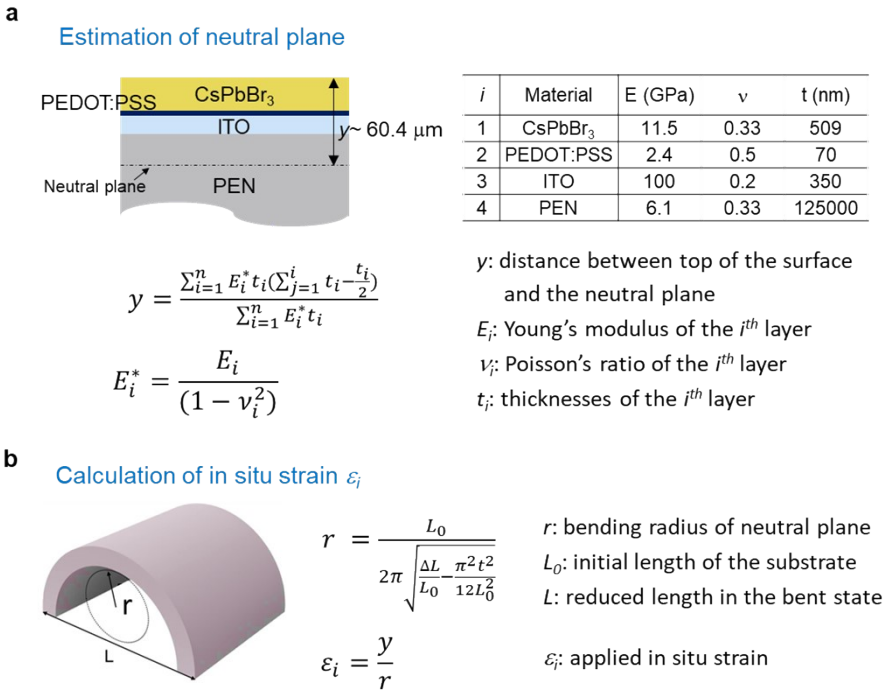

Fig. S1. Estimation procedure of (a) neutral plane and (b) in situ strain ε_i, according to the equations used for the estimation with the definitions of parameters.

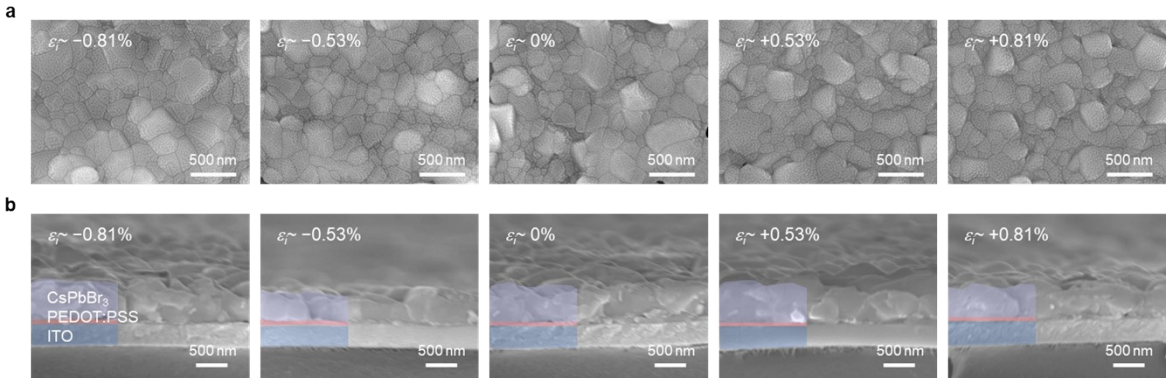

Fig. S2. (a) Surface SEM images and (b) cross-sectional images of $CsPbBr_3$ thin films processed with in situ strain ε_i from –0.81% to +0.81%.

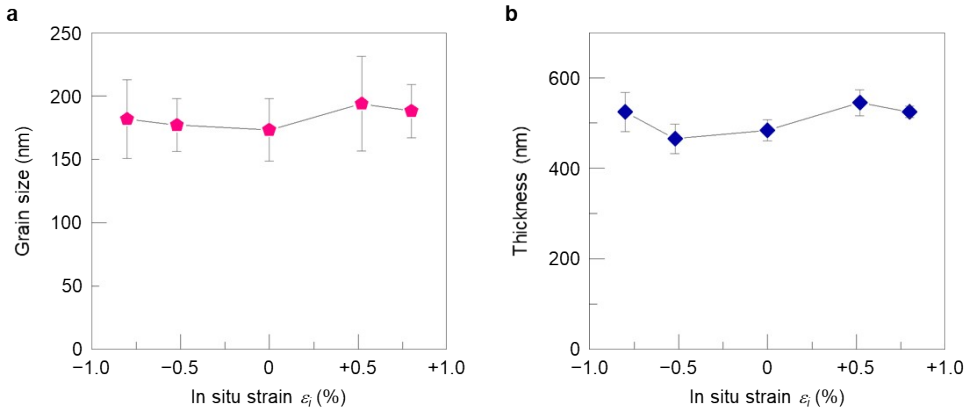

Fig. S3. Variations in (a) average grain size and (b) thickness of the $CsPbBr_3$ thin films processed with in situ strain ε_i from –0.81% to +0.81%.

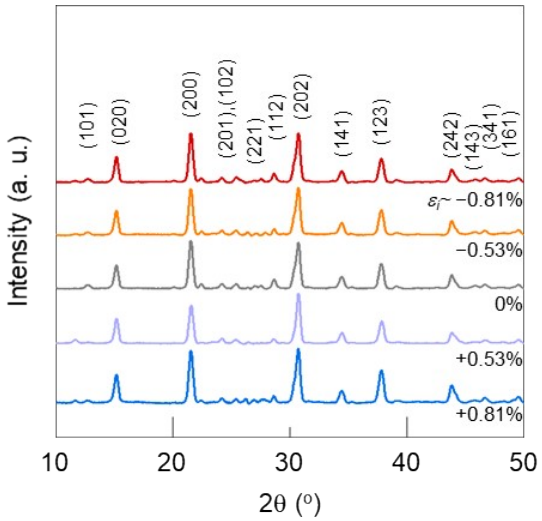

Fig. S4. HR-XRD patterns of the $CsPbBr_3$ thin films processed with different in situ strain.

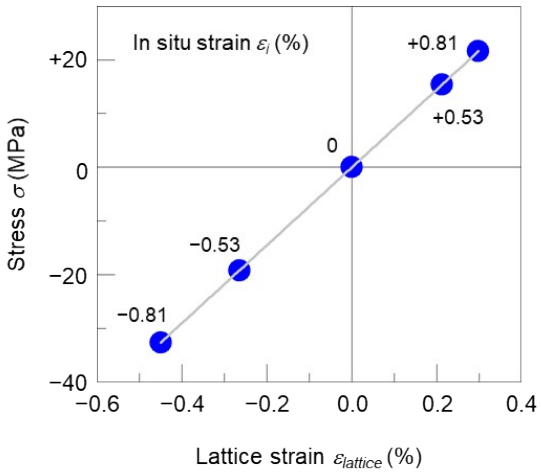

Fig. S5. Dependence of in situ strain ε_i with the estimated stress σ for the strained $CsPbBr_3$ thin films. Here, σ was calculated according to the biaxial strain model using the following equation[1] of $\sigma = \left[2C_{13} - C_{33}\frac{(C_{11}+C_{12})}{C_{13}}\right]\frac{(b-b_0)}{b_0}$, where C_{ij} is the elastic stiffness constant of $CsPbBr_3$ (i and j = 1, 2 or 3),[2] and b and b_0 are the lattice constants for the strained and unstrained films, respectively.

Reference

1. Choi, H.J., Jung, Y.S., Han, J., and Cho, Y.S. (2020). In-situ stretching strain-driven high piezoelectricity and enhanced electromechanical energy-harvesting performance of a ZnO nanorod-array structure. Nano Energy 72, 104735.

2. Lee, J.H., Deng, Z., Bristowe, N.C., Bristowe, P.D., and Cheetham, A.K. (2018). The competition between mechanical stability and charge carrier mobility in MA-based hybrid perovskites: Insight from DFT.J. Mater. Chem. C 6, 12252-12259.

Table S1. Structural information of the strained $CsPbBr_3$ thin films, which were extracted from the HR-XRD results.

In situ strain ε_i (%)	Lattice constant (Å)			Volume V (Å^3)	ΔV (%)	Stress σ (MPa)
	a	b	c			
−0.81	8.24607	11.67378	8.25939	795.07	−0.72	−32.6
−0.53	8.25939	11.69552	8.25718	797.63	−0.40	−19.2
0	8.27340	11.72634	8.25475	800.85	0.00	0.0
+0.53	8.28594	11.75148	8.25368	803.68	0.35	15.4
+0.81	8.29118	11.76146	8.25358	804.86	0.50	21.6

Table S2. Estimated values of strain field over 25-mm-long $CsPbBr_3$ thin films, which depend on the applied in situ strain ranging from −0.81% to +0.81%.

In situ strain (%) / x-position (mm)	−0.81	−0.53	0	+0.53	+0.81
0	0.00	−0.00	0.00	0.00	0.00
0.5	−0.03	−0.02	0.00	0.02	0.03
1	−0.07	−0.04	0.00	0.04	0.07
1.5	−0.10	−0.07	0.00	0.07	0.10
2	−0.12	−0.09	0.00	0.09	0.12
2.5	−0.16	−0.11	0.00	0.11	0.16
3	−0.19	−0.13	0.00	0.13	0.19
3.5	−0.22	−0.14	0.00	0.14	0.22
4	−0.26	−0.16	0.00	0.16	0.26
4.5	−0.29	−0.19	0.00	0.19	0.29
5	−0.32	−0.21	0.00	0.21	0.32
5.5	−0.35	−0.23	0.00	0.23	0.35
6	−0.38	−0.25	0.00	0.25	0.38
6.5	−0.41	−0.27	0.00	0.27	0.41
7	−0.45	−0.29	0.00	0.29	0.45
7.5	−0.48	−0.32	0.00	0.32	0.48
8	−0.51	−0.34	0.00	0.34	0.51
8.5	−0.55	−0.36	0.00	0.36	0.55
9	−0.57	−0.38	0.00	0.38	0.57
9.5	−0.60	−0.40	0.00	0.40	0.60
10	−0.64	−0.42	0.00	0.42	0.64
10.5	−0.68	−0.44	0.00	0.44	0.68
11	−0.71	−0.47	0.00	0.47	0.71
11.5	−0.74	−0.49	0.00	0.49	0.74
12	−0.78	−0.51	0.00	0.51	0.78
12.5	−0.81	−0.53	0.00	0.53	0.81
13.0	−0.78	−0.51	0.00	0.51	0.78
13.5	−0.74	−0.49	0.00	0.49	0.74
14.0	−0.71	−0.47	0.00	0.47	0.71
14.5	−0.68	−0.44	0.00	0.44	0.68
15	−0.64	−0.42	0.00	0.42	0.64
15.5	−0.60	−0.40	0.00	0.40	0.60
16	−0.57	−0.38	0.00	0.38	0.57
16.5	−0.55	−0.36	0.00	0.36	0.55
17	−0.51	−0.34	0.00	0.34	0.51
17.5	−0.48	−0.32	0.00	0.32	0.48
18	−0.45	−0.29	0.00	0.29	0.45
18.5	−0.41	−0.27	0.00	0.27	0.41
19	−0.38	−0.25	0.00	0.25	0.38
19.5	−0.35	−0.23	0.00	0.23	0.35
20	−0.32	−0.21	0.00	0.21	0.32
20.5	−0.29	−0.19	0.00	0.19	0.29
21	−0.26	−0.16	0.00	0.16	0.26
21.5	−0.22	−0.14	0.00	0.14	0.22
22	−0.19	−0.13	0.00	0.13	0.19
22.5	−0.16	−0.11	0.00	0.11	0.16
23	−0.12	−0.09	0.00	0.09	0.12
23.5	−0.10	−0.07	0.00	0.07	0.10
24	−0.07	−0.04	0.00	0.04	0.07
24.5	−0.03	−0.02	0.00	0.02	0.03
25	0.00	0.00	0.00	0.00	0.00

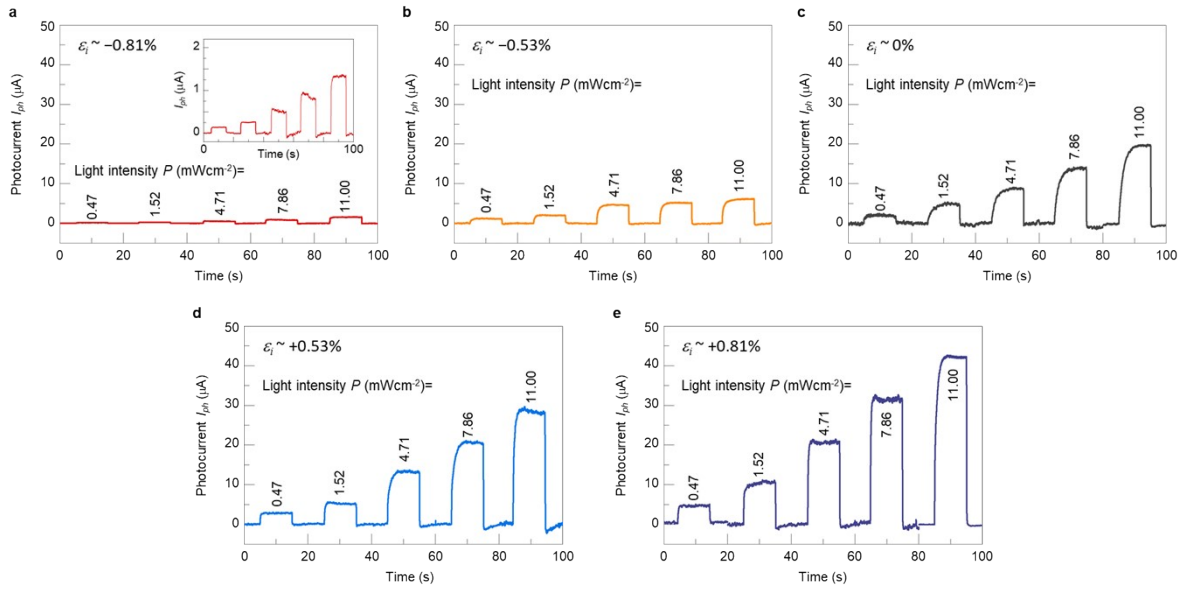

Fig. S6. Photocurrent-time behavior for photodetectors based on the strained $CsPbBr_3$ thin films under various light intensities from 0.47 to 11.0 $mWcm^{-2}$.

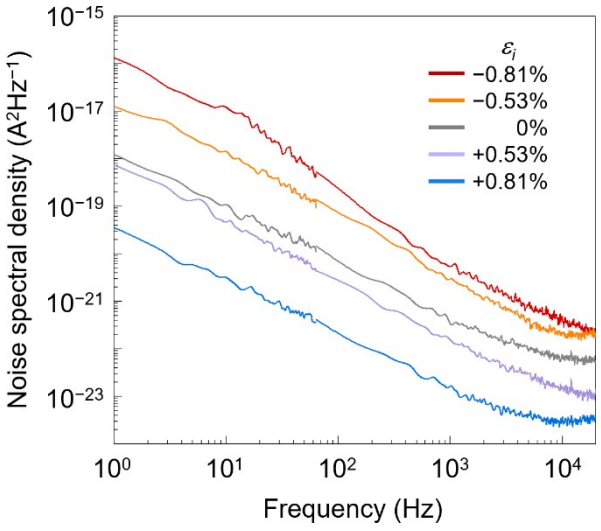

Fig. S7. Noise spectral density as a function of frequency for the strained $CsPbBr_3$ photodetectors.

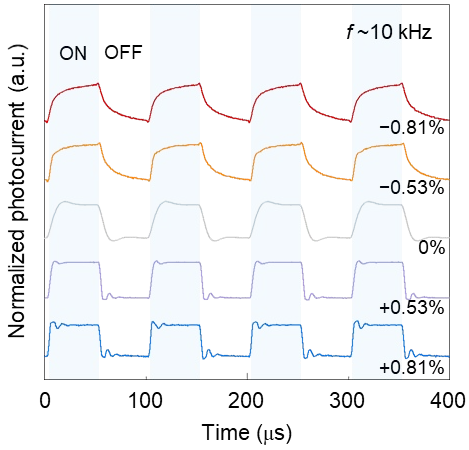

Fig. S8. Normalized photoresponse curves obtained at a fixed frequency of 10 kHz using a 470 nm-light source for the strained $CsPbBr_3$ photodetectors.

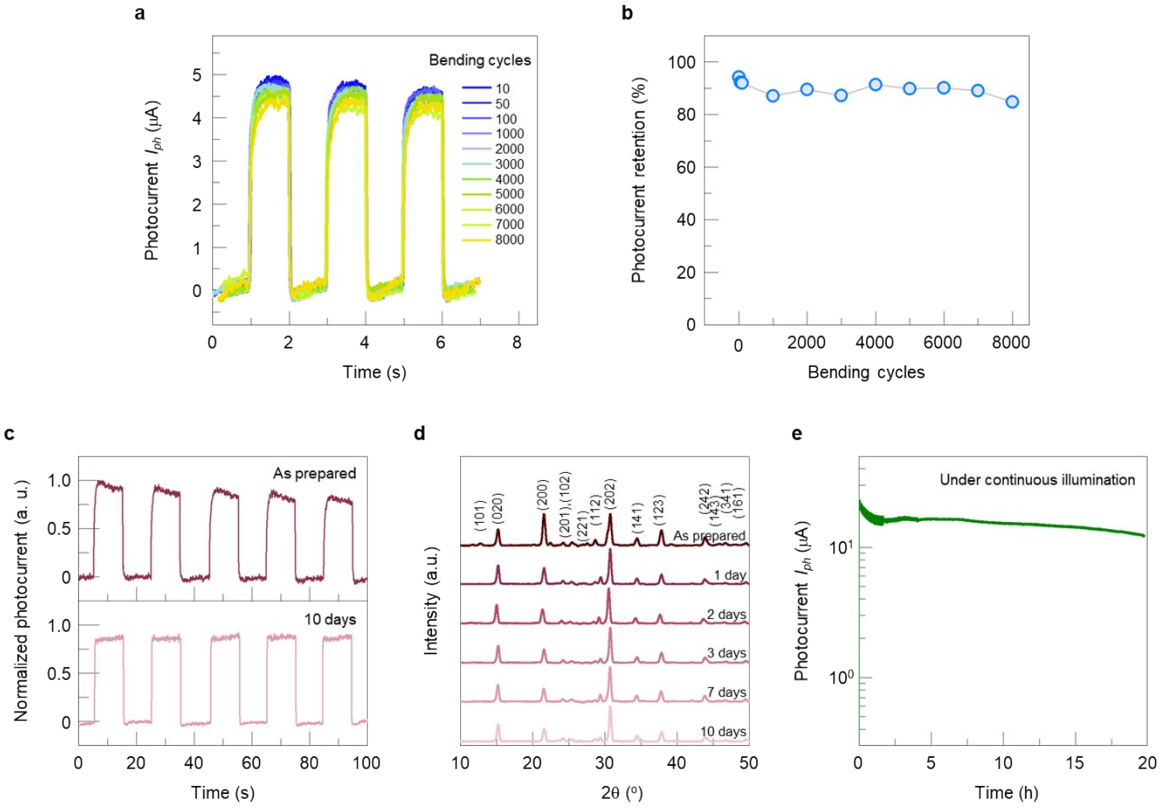

Fig. S9. (a) The photocurrent I_{ph}-time behavior of the +0.81%-strained $CsPbBr_3$ photodetector after repetitive bending up to 8000 cycles at a compressive bending strain of ~1.01%, (b) photocurrent retention compared to the initial I_{ph} with the progress of bending operation up to 8000 cycles, (c) normalized photocurrent-time and (d) HR-XRD patterns of the +0.81%-strained $CsPbBr_3$ photodetector after atmosphere exposure for 10 days at room temperature with a relative humidity of 60±5%, and (e) the photocurrent detected with the extended time of 20 h under the continuous light illumination at 4.71 $mWcm^{-2}$ for the +0.81%-strained $CsPbBr_3$ photodetector.

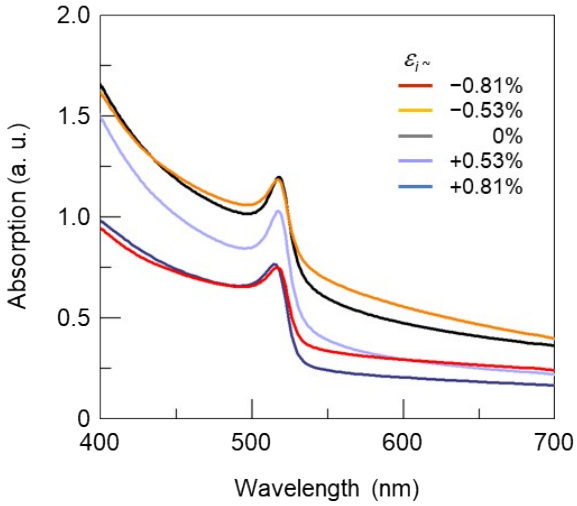

Fig.S10. Absorption spectra of the $CsPbBr_3$ thin films processed with in situ strain ε_i ranging from –0.81% to +0.81%.

Table S3. Energy band levels with respect to the vacuum level as determined by the UPS spectra (here, SECO is the secondary electron cut-off region, E_F is the Fermi level, LBE is the low binding energy, E_v is the valence band edge, E_g is the optical energy bandgap, and E_c is the conduction band edge)

In situ strain ε_i (%)	SECO	E_F	LBE	E_v	E_g	E_c
−0.81	17.408	−3.792	1.80	−5.592	2.317	−3.275
−0.53	17.203	−3.997	1.85	−5.847	2.324	−3.523
0	17.163	−4.037	1.90	−5.937	2.328	−3.609
+0.53	17.077	−4.123	1.95	−6.073	2.336	−3.737
+0.81	16.916	−4.284	2.00	−6.284	2.340	−3.944

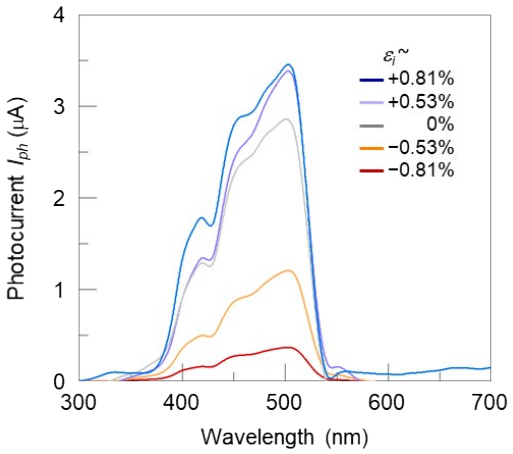

Fig. S11. Photocurrent as a function of incident wavelength for the strained $CsPbBr_3$ photodetectors.

Table S4. Estimated variations of crystal-structural attributes in the perovskite $CsPbBr_3$ structure for the different in situ strain ε_i ranging from –0.81% to +0.81%.

In situ strain ε_i (%)	−0.81	−0.53	0	+0.53	+0.81
Average Pb–Br bond length (Å)	2.9681	2.9713	2.9753	2.9787	2.9802
$PbBr_6$ octahedron volume (Å^3)	34.8599	34.9718	35.1131	35.2372	35.2890
Pb–Br–$Pb_{equatorial}$ bond angle (°)	164.3206	164.3530	164.3977	164.4322	164.4453
Pb–Br–Pb_{apical} bond angle (°)	156.6900	156.6833	156.6724	156.6643	156.6613

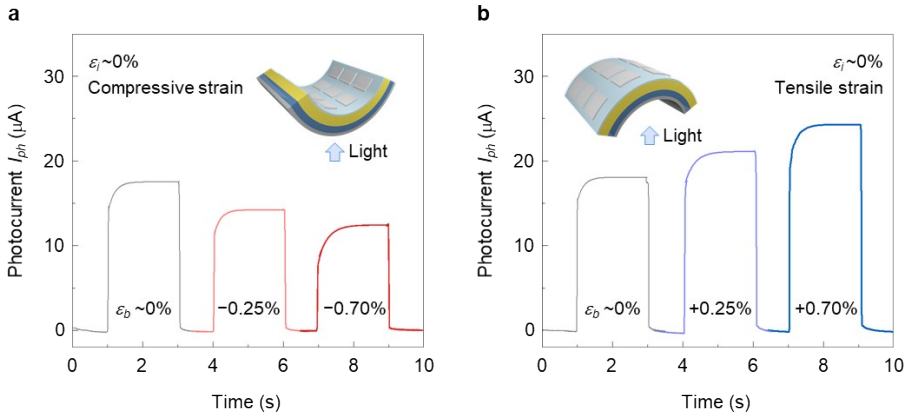

Fig. S12. Time-dependent photoresponse of the photodetectors processed with no in situ strain, but subject to post-bending in either (a) concave or (b) convex manner to create compressive or tensile strain, respectively. The photocurrent was measured at the light intensity P of 11.0 mW/cm^2 in the state of the post-bending.